SANDIA REPORT

SAND2001-0836
Unlimited Release
Printed April 2001

Formation of Random, RIE-Textured Silicon Surfaces with Reduced Reflection and Enhanced Near IR Absorption

Saleem H. Zaidi

Prepared by
Sandia National Laboratories
Albuquerque, New Mexico 87185 and Livermore, California 94550

Sandia is a multiprogram laboratory operated by Sandia Corporation, a Lockheed Martin Company, for the United States Department of Energy under Contract DE-AC04-94AL85000.

Sandia National Laboratories

Issued by Sandia National Laboratories, operated for the United States Department of Energy by Sandia Corporation.

Available to DOE and DOE contractors from
U.S. Department of Energy
Office of Scientific and Technical Information
P.O. Box 62
Oak Ridge, TN 37831

Telephone: (865)576-8401
Facsimile: (865)576-5728
E-Mail: reports@adonis.osti.gov
Online ordering: http://www.doe.gov/bridge

Available to the public from
U.S. Department of Commerce
National Technical Information Service
5285 Port Royal Rd
Springfield, VA 22161

Telephone: (800)553-6847
Facsimile: (703)605-6900
E-Mail: orders@ntis.fedworld.gov
Online order: http://www.ntis.gov/ordering.htm

SAND2001-0836
Unlimited Release
Printed April 2001

FORMATION OF RANDOM, RIE-TEXTURED SILICON SURFACES WITH REDUCED REFLECTION AND ENHANCED NEAR IR ABSORPTION

Saleem H. Zaidi
Gratings, Inc.
2655-A Pan American Fwy., NE
Albuquerque, NM 87107

CONTRACT # BE-8229
JANUARY 1 TO SEPTEMBER 30, 2000

ABSTRACT

We have developed novel metal-assisted texturing processes that have led us to optically favorable surfaces for solar cells. Large area (~ 200 cm^2) uniform texturing has been achieved. The physical dimensions of the chamber limited texturing of even larger wafers. Surface contamination and residual RIE-induced damage were removed by incorporation of a complete RCA clean process followed by wet-chemical etching treatments. RIE-textured solar cells with optimized profiles providing performance comparable to the random, wet-chemically etched cells have been demonstrated. A majority of the texture profiles exhibit an enhanced IQE response in the near IR region. Using scanning electron microscope measurements, we carried out a detailed analysis of the microstructure of random RIE-textured surfaces. The random microstructure represents a superposition of sub-μm grating structures with a wide distribution of periods, depths, and profiles as determined by the SEM measurements. These structures were modeled using GSOLVER™ software for periodic patterns. The enhanced IR response from random, RIE-textured surfaces is attributed to enhanced coupling of light into the transmitted diffraction orders. These obliquely propagating diffraction orders generate electron-hole pairs closer to the surface, thus, reducing bulk recombination losses relative to a non-scattering, planar surface with identical hemispherical reflection. The optimized texture and damage removal processes have been applied to large area (100-132 cm^2) multi-crystalline wafers. Initial results have demonstrated improved performance relative to planar, control wafers. However, the texture and solar cell fabrication processes require further optimization in the RCA clean, DRE treatments, and emitter formation in order to fully realize the benefits of the low-reflection (~ 1-2 %) textured surface.

TABLE OF CONTENTS

1. INTRODUCTION

Reducing reflection losses by a mechanism that can simultaneously enhance its near IR absorption significantly increases the performance of a Si solar cell [1]. In a weakly absorptive isotropic medium of refractive index n, statistical analysis shows that the absorption in a textured surface can be enhanced by as much as $4n^2$ in comparison with a planar surface [2]. Deckmann, et al. [3] have shown that this statistical limit is reached for average feature dimensions comparable to the wavelength of light inside the medium. If texture dimensions are too large compared to the optical wavelengths, the light is specularly reflected without achieving optimum random scattering. If texture dimensions are too small compared to wavelength, light scattering is ineffective due to an inability to resolve the microstructure. Therefore, the ability to control the microstructure dimensions is critical for improving solar cell performance.

The random, reactive ion etching (RIE) texturing techniques described here provide a controllable approach aimed at scaling randomly etched features. This tunability enables us to achieve enhanced absorption without incurring reflection losses. These texturing techniques are also attractive due to their applicability to low-cost, large area multi-crystalline Si wafers. Texturing of mc-Si is a field of active research due to the inability to find a reliable texturing process that combines low-reflection with enhanced near IR absorption. Several techniques including anodic etching [4], mechanical texturing [5], and multi-layer anti-reflection films are being investigated. The random, RIE-texturing with controllability over feature dimensions is potentially attractive due to low-cost, high-throughput, and adaptability to large areas.

1a. METAL-ASSISTED RANDOM RIE-TEXTURING OF SILICON

In a typical random RIE-texturing process, nanoscale metal particles either from the chamber walls, or from a suitable source are introduced into the plasma during the etching process. These particles are randomly deposited on the Si surface, and act as " micromasks" [6]. These randomly distributed micromasks protect Si underneath from etching, while rest of the unprotected regions is etched. As a result, the random texturing of Si is achieved.

Using 790-Plasma-Therm RIE system, we have investigated a wide process range consisting of SF_6, O_2, CF_4, CHF_3 gases, their flow rates, chamber pressures, RF power, dc Bias, and substrate temperature. We were able to achieve consistent, reproducible texturing under certain conditions using SF_6/O_2 plasma chemistry [7]. We determined that the texture process was strongly influenced by various metal sources introduced into the reaction chamber. The catalytic behavior of metals in texturing different profiles is critically important in determining an optically favorable textured surface for solar cells as discussed earlier. Figure 1 shows hemispherical reflectance measurements from various metal-assisted texturing processes. For comparison, we have also shown the reflectance from conventional, random wet-chemically textured and planar Si surfaces. Spectral reflectance measurements were carried out at Sandia National Laboratories using a Cary Model 5E (UV-VIS-NIR) spectrophotometer and a labsphere (RSA-CA-50) integrating sphere. These measurements show that Ti and Cr-assisted processes achieve the lowest reflection, whereas the Pd-assisted process leads to the highest reflection. Figure 2 shows the SEM profiles of Cr, Ti, and Pd-assisted textured surfaces. There is a wide distribution of feature sizes, profiles, and depths. The Cr-assisted textured features are typically ~ 50-100 nm in diameter and separation with ~ 100-500-nm depths. The low-reflection from such profiles is most likely due to graded-index behavior of the textured region [8]. The Ti-assisted profiles combine ~ 50-100-nm ridges at the top of ~ 1-μm deep trenches with typical hole-diameters ranging from ~ 500-1000 nm. Diffractive scattering effects probably cause the low reflection from such surfaces [9]. Finally, the Pd-assisted texture has dimensions > 1-2 μm, and light interaction is dominated by specular scattering.

We have also observed that the texture uniformity over the wafer and its microstructure are both critically influenced by the manner of introduction of the metal sources. Figure 3 shows the reflectance measurements from two surfaces that were textured identically except for using different methods of Al-source introduction. It is

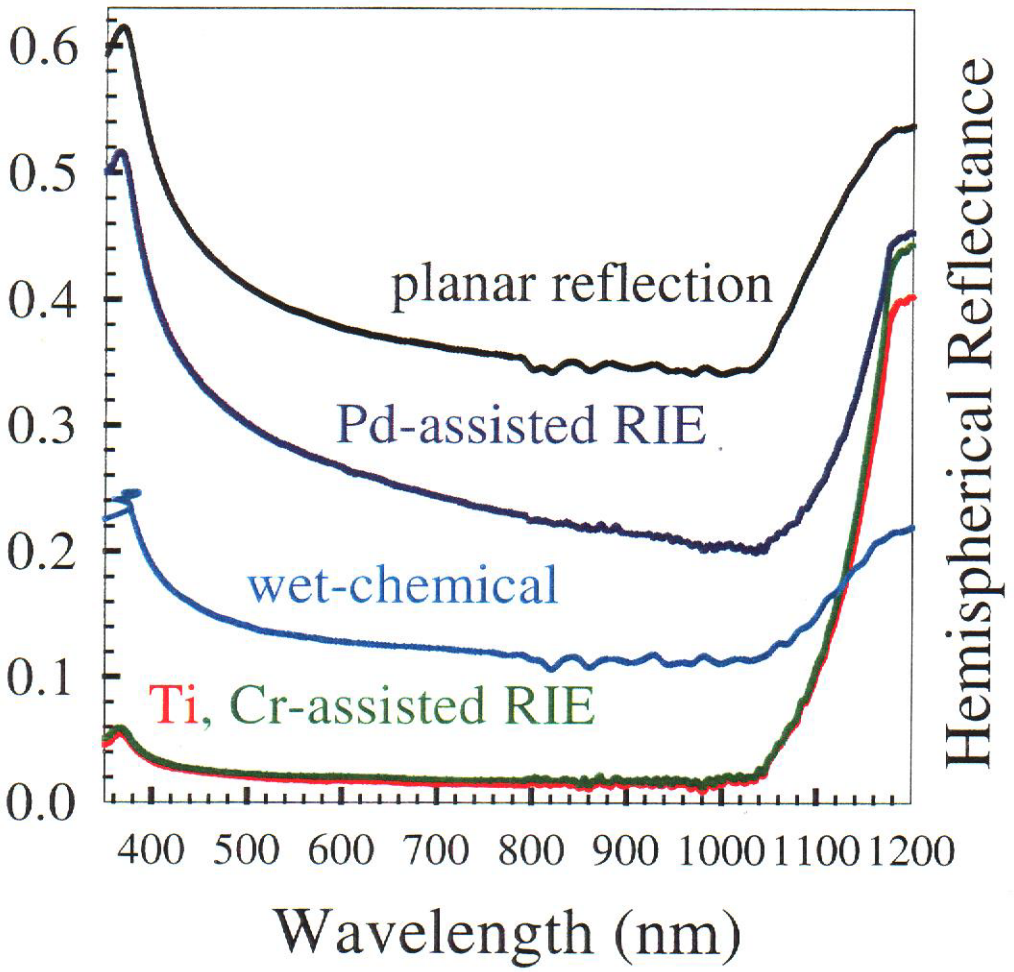

Figure 1. Hemispherical reflectance measurements from various metal-assisted random RIE-textured surfaces. Also plotted for comparison are reflectances of wet-chemical texture-etched and planar surfaces.

seen that reflection is significantly lower for method 2. Figure 4 shows the SEM pictures of the microstructure for the two cases. It is seen that microstructure changes from columnar (50-100 nm diameter, ~ 1-μm deep) to several μm wide features with extremely thin ridges. Finally, Figure 5 shows reflectance measurements from three other texture processes. The cathode-1 process refers to etching of Si wafers on one type of cathode, instead of another type-2 cathode. The hybrid texture process refers to etching sequentially on both types of cathodes, and finally the conditioned texture process refers to an un-assisted texturing process in which the chamber is first conditioned prior to texture-etching wafers. The SEM profiles of hybrid and conditioned textures are shown in Figure 6. The hybrid texture is somewhat similar to the Ti-assisted texture process, whereas the conditioned texture is similar to Cr-assisted textures, except that the feature dimensions are approximately an order of magnitude larger. The cathode-1 textures, not shown in Figure 6, are similar to Cr-assisted profiles.

In summary, we have developed novel, metal-assisted texturing processes that lead to a wide range of etched profiles and reflectance responses. A detailed understanding of the plasma processes is required to understand the underlying physical mechanisms. It appears that the variation in texture profiles is due to different sputtering rates of various metal sources.

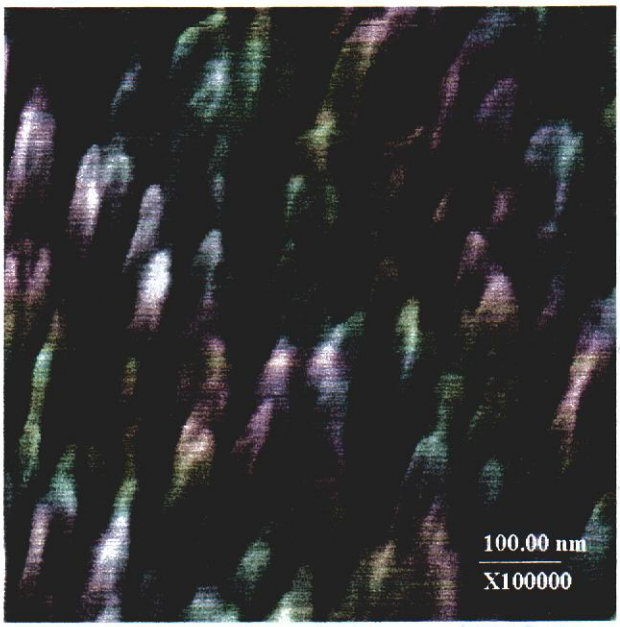

Cr-assisted

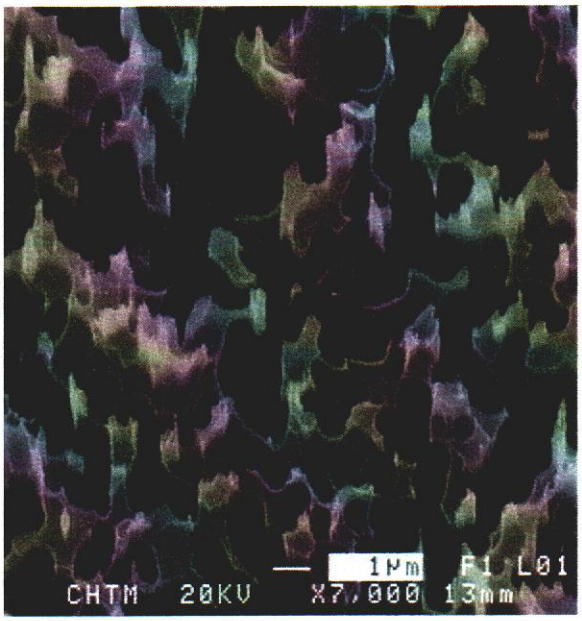

Pd-assisted

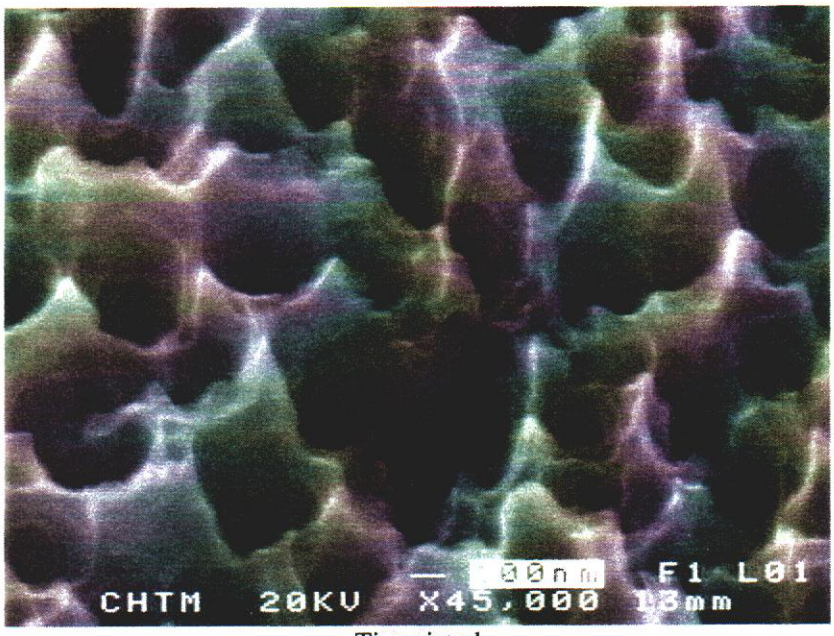

Ti-assisted

Figure 2. SEM pictures of Cr, Pd, and Ti-assisted RIE-textured surfaces. The white lines represent length scales of 100-nm for Cr & Ti-assisted textured surfaces, and 1-µm for Pd-assisted.

2. SOLAR CELL FABRICATION

Details of the solar cell fabrication are given in reference [9]. All solar cells were fabricated on 4" diameter p-type (~ 1-2 Ω cm) Si wafers. Si wafers were RIE-textured, cleaned using complete RCA treatment followed by the damage removal wet-chemical etching treatments. The junctions were formed using a $POCl_3$ gas diffusion process. For comparison, a region of ~ $4cm^2$ was protected from RIE etching to provide a planar reference. All cells had a 70-nm anti-reflection, PECVD-nitride film.

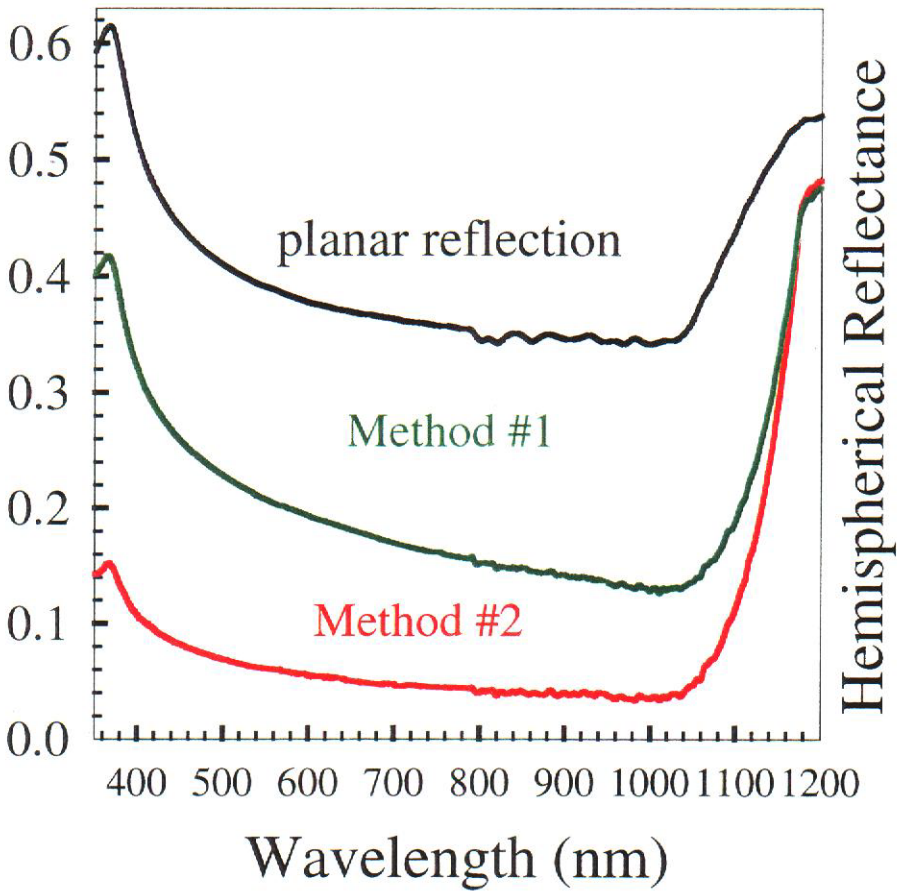

Figure 3. Hemispherical reflectance measurements from Al-assisted random RIE-textured surfaces.

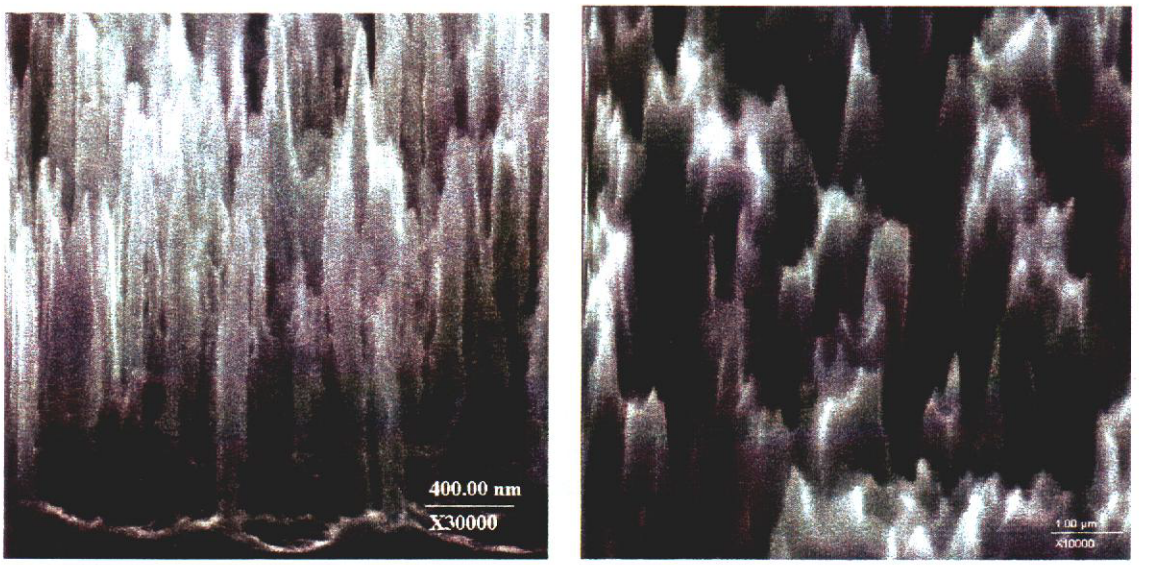

Figure 4. SEM pictures of Al-assisted RIE-textured surfaces, method # 1 (left), method # 2 (right).

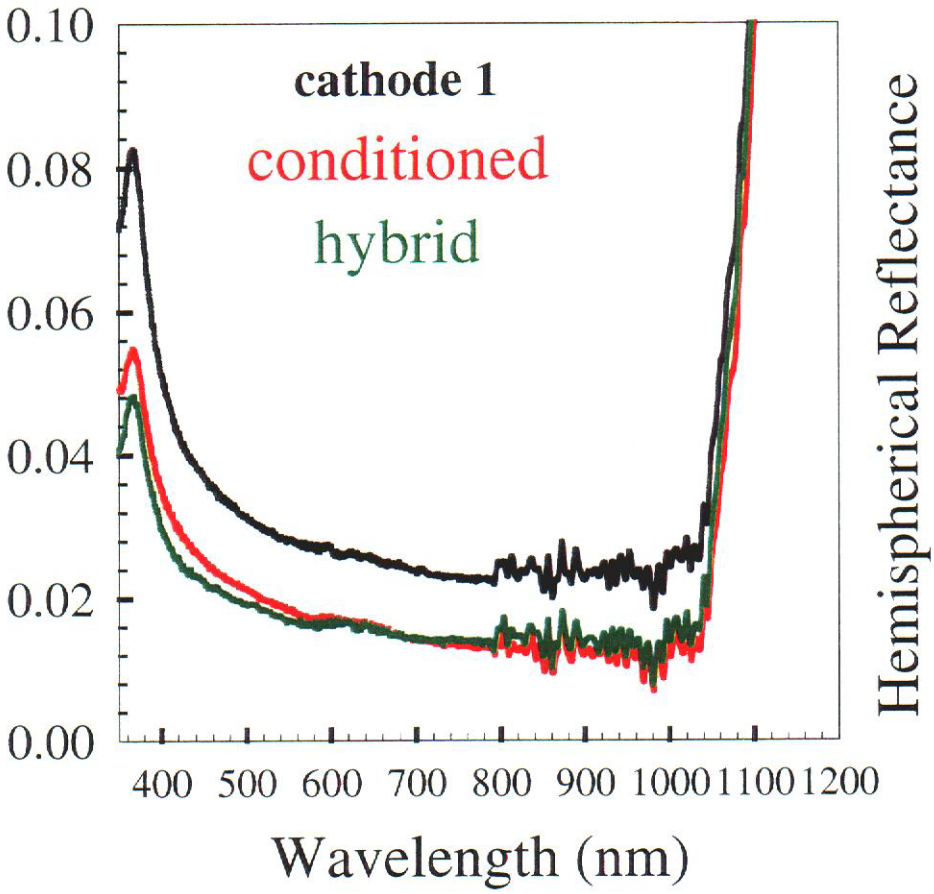

Figure 5. Hemispherical reflectance measurements from un-assisted random RIE-textured surfaces.

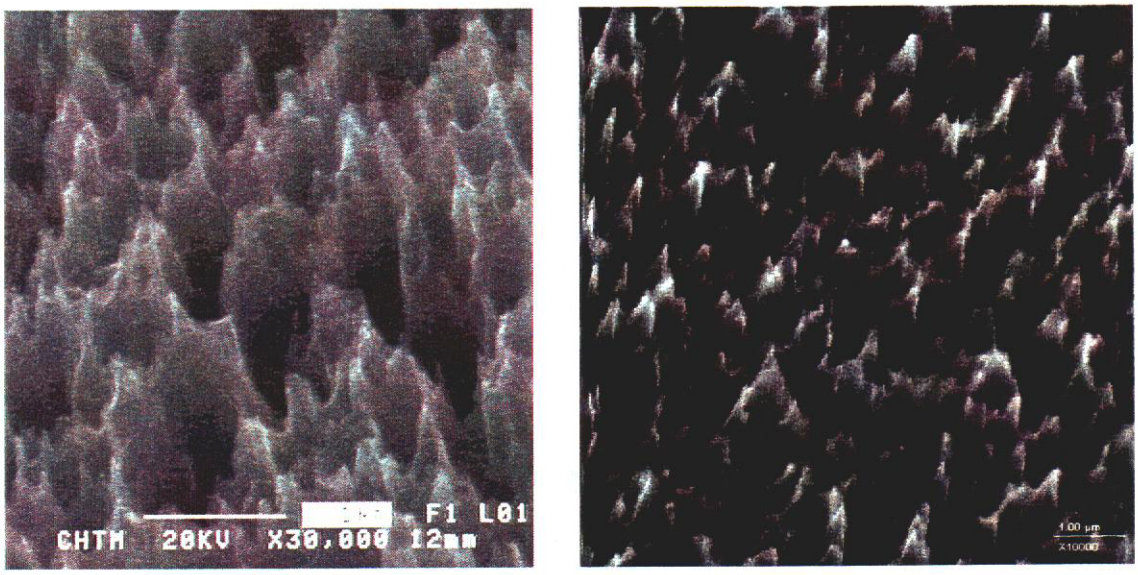

Figure 6. SEM pictures of hybrid (left) and conditioned (right) RIE-textured surfaces.

3. INTERNAL QUANTUM EFFICIENCY MEASUREMENTS

Internal quantum efficiency (IQE) measurements provide an accurate tool for characterization of solar cell performance [9]. We can use IQE measurements to evaluate the influence of the surface texture over solar cell performance. In order to isolate variations in bulk material properties, IQEs are measured from the adjacent planar and textured regions of each individual solar cell. Texture IQEs from different wafers are meaningful only if their respective planar region IQEs are nominally identical. The IQE, efficiency, and reflectance responses of solar cells textured with six different processes are discussed in the following three sub-sections.

3a. TEXTURING ON CATHODE-1

The cathode-1 texturing process has been described earlier in section 1. Here we present solar cell performance from these textures. Figure 7 shows IQE and hemispherical reflectance measurements as a function of RIE etch time, for comparison IQE from a planar surface is also plotted. We notice that spectral reflectance is relatively insensitive to etch time variation. Similarly, we notice that for both 6 and 10-min etch times, IQEs are almost identical, significantly higher IQE is observed for the 14-min etch time. Notice that the IQEs for all three cases are significantly reduced in comparison with the planar surface over the entire spectral range presumably due to residual surface damage. Figure 8 shows SEM pictures of the random RIE textured profiles for each of the three etch times. A comparison of the etched structures shows that increase in etch time reduces texture density leaving relatively larger features at longer etch times. The randomly etched features support etch depth varying from ~ 0.5-1.5-μm in all three cases.

In order to improve IQE response, we have investigated various damage removal etch (DRE) treatments [9]. Figure 9 shows planar and textured hemispherical reflectance and IQE responses of the 14-min RIE texturing process that was followed by a 270-sec KOH DRE aimed at recovering a damage-free Si surface. Also

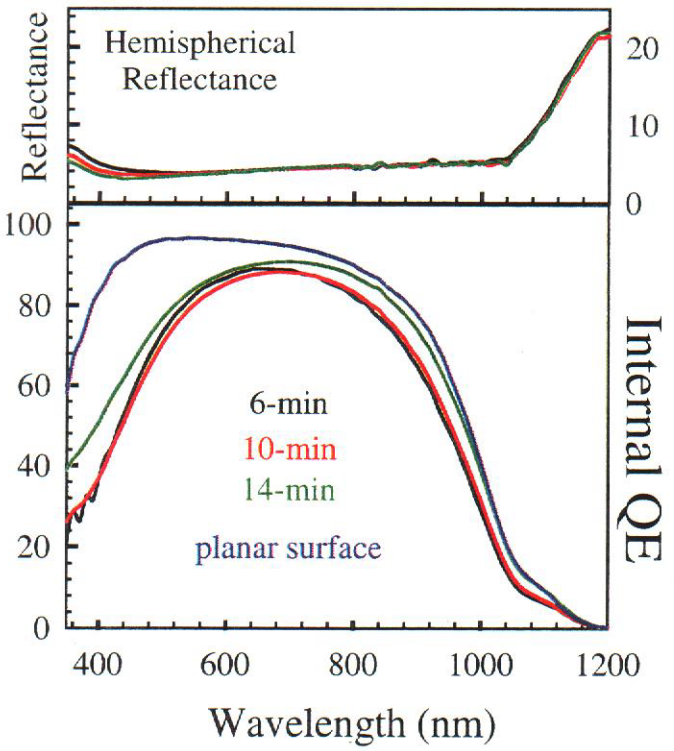

Figure 7. IQE and hemispherical reflectance measurements as a function of RIE etch time.

Figure 8. SEM pictures of random RIE textured profiles as a function of etch time, the length scale on all three SEM pictures is 0.8 μm.

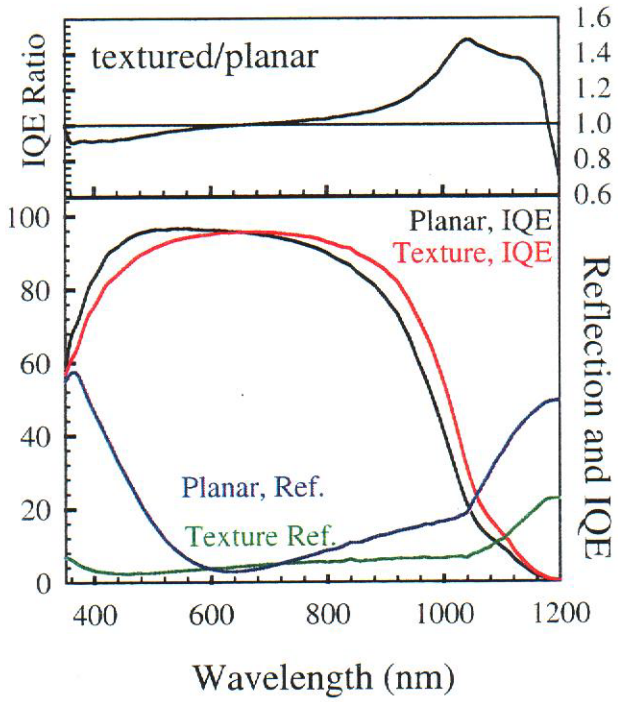

Figure 9. IQE, hemispherical reflectance and IQE ratio measurements for planar and KOH-treated 14-min RIE-textured surfaces.

plotted in Figure 9 is the IQE ratio of textured to the planar regions of the same wafer. A comparison of planar and textured surface responses in Figure 9 shows that the KOH treatment has significantly improved textured IQE response over the entire spectral range. However, the texture IQE is lower than the planar in the 350-650-nm spectral region. In the long wavelength spectral region ($\lambda > 650$ nm), the texture IQE is higher with a maximum ratio of ~ 1.5 at λ=1.0 μm. The solar-weighted surface reflectance of the textured surface at 4.5 % is significantly lower than the planar surface reflection of ~ 11.8 %, and is comparable to the 14-min RIE surface reflectance of ~ 4.2 %. Figure 10 shows the SEM pictures of the KOH-treated random RIE-textured surface. It is seen that KOH etch has almost etched off the fine features, i.e., etched features in ~ 50-100-nm range. Also, overall separation between random features has increased without causing significant variations in etched depths.

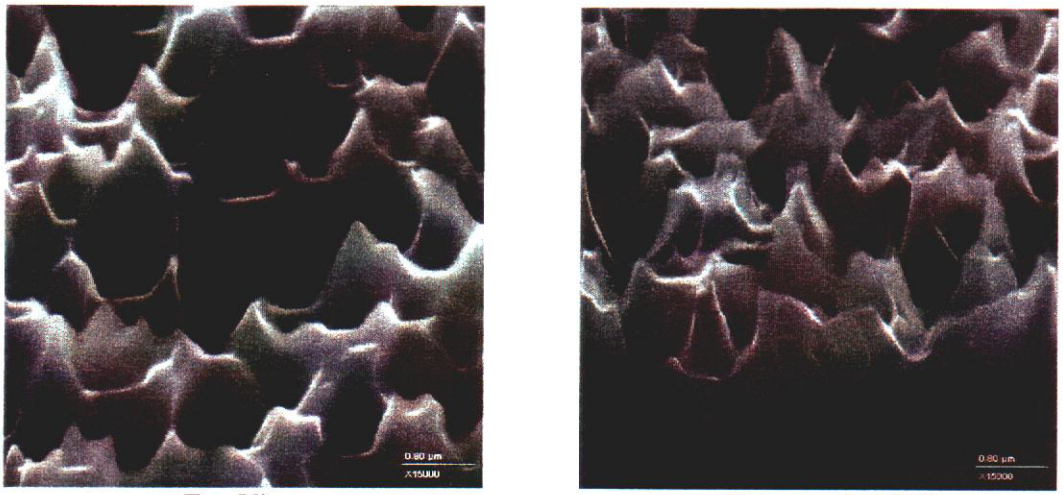

Top View Cross-sectional View

Figure 10. SEM pictures of 14-min random RIE textured profiles followed by 270-sec KOH etch, the length scale on both SEM pictures is 0.8 μm.

For the 14-min etch process, we have also evaluated DRE with nitric acid solution [9]. Figure 11 shows the IQE and reflectance measurements of the planar and textured surfaces. Planar and textured IQE comparison in Figure 11 shows the texture IQE is lower than the planar in 350-600-nm spectral region. At long wavelengths, the texture IQE is higher with a maximum of ~ 1.3 at λ ~ 1150 nm. The solar-weighted reflectance from nitric-etched surface at ~ 5.5 % is slightly higher than the KOH-treated surface. Figure 12 shows the SEM pictures of the nitric DRE random RIE-textured surface. It is seen that nitric DRE has etched all the nanoscale features, also the typical

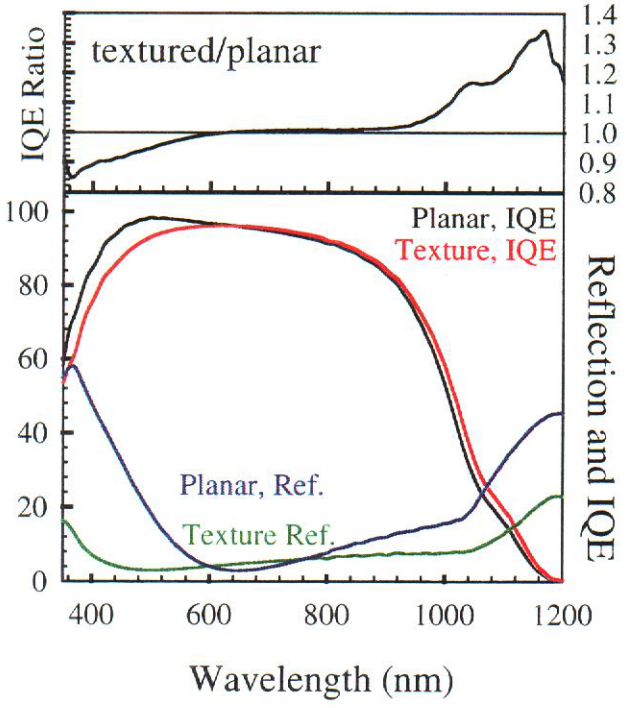

Figure 11. IQE, hemispherical reflectance and IQE ratio measurements for planar and nitric-treated 14-min RIE-textured surfaces.

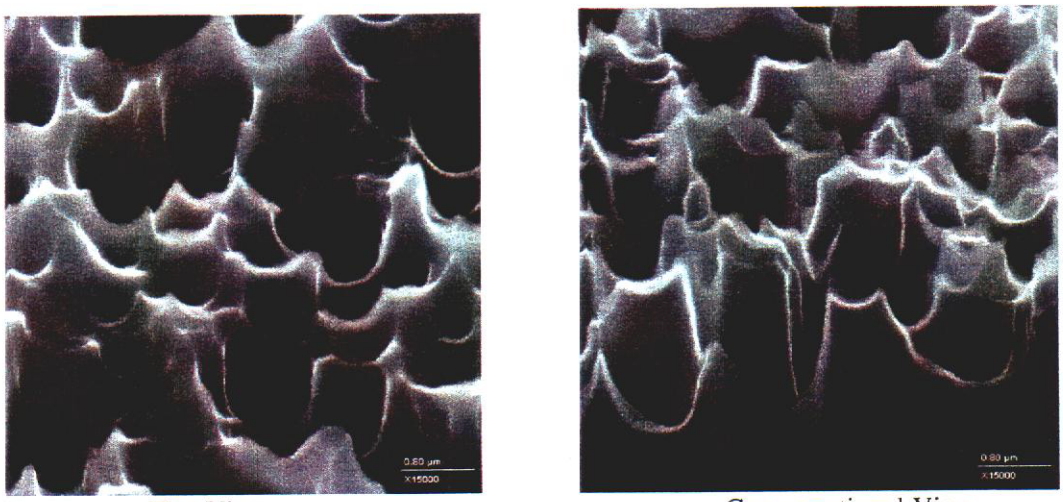

Top View Cross-sectional View

Figure 12. SEM pictures of 14-min random RIE textured profiles followed by 15-sec nitric etch, the length scale on both SEM pictures is 0.8 μm.

separation between individual features has increased to ~ 0.5-1.0 μm. Finally, in Figure 13, we have plotted I-V measurements under one-sun illumination for the five cells shown in Figures 7, 9, & 11. Table 1 summarizes some of the critical cell parameters. Comparison of cell parameters in table 1 shows that the cell efficiencies and short-circuit currents increase as etch times are increased, while the open-circuit voltages and fill factors remain constant. The KOH and nitric DREs produce significant improvements in short-circuit currents. For the KOH DRE, open-circuit voltage has improved significantly, whereas nitric DRE does not show the same improvement. For both DREs, fill factors are much lower, which is perhaps responsible for lower cell efficiencies.

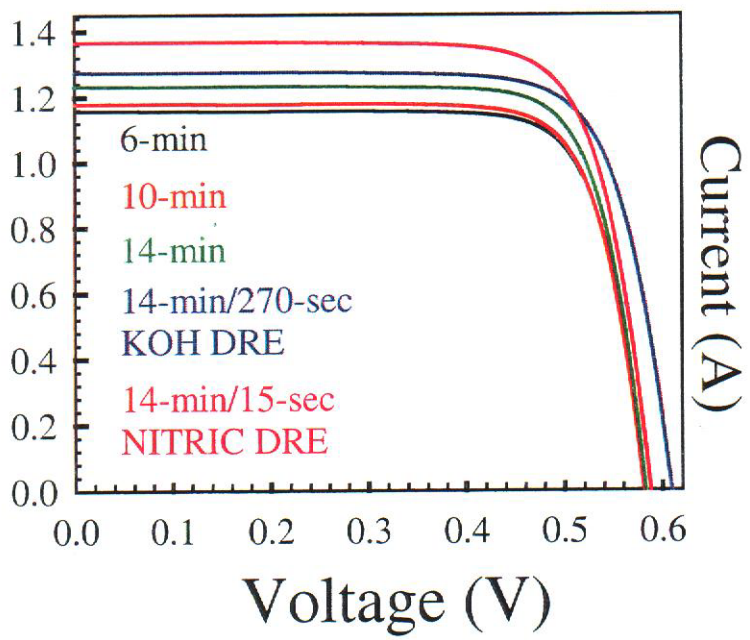

Figure 13. I-V measurements under one-sun illumination for the random RIE textured, KOH and nitric-etched solar cells.

Table 1. SOLAR CELL PARAMETERS OF SILICON CATHODE TEXTURE WITH AND WITHOUT DREs

Cell description	Efficiency (%)	Open-circuit voltage (V)	Short-circuit current (A)	Fill factor
6-min RIE	12.7	0.582	1.162	0.785
10-min RIE	14.73	0.581	1.174	0.781
14-min RIE	15.31	0.583	1.235	0.783
14-min RIE+270-sec KOH	15.27	0.609	1.273	0.764
14-min RIE+15-sec NITRIC	14.74	0.588	1.378	0.765

3b. ALUMINUM-ASSISTED TEXTURING ON CATHODE-2

The Al-assisted texturing process has been described earlier in section 1. Here we present solar cell performance from this texture process. Figure 14 shows IQE and hemispherical reflectance measurements as a function of RIE etch time. We notice that for this texture process, spectral reflectance is relatively insensitive to etch times of 6 and 10 minutes. For the 14-minute etch time, the hemispherical reflection is significantly increased in the short wavelength region. For this texture, the 6-min IQE is superior to 10-min in the short wavelength region, the higher long wavelength response of the 10-min. etch is due to improved bulk properties of this wafer. The IQE response of the 14-min etch is superior to shorter etch times, however, the overall IQE is still lower than the planar surface. Figure 15 shows SEM pictures of random RIE textured profiles for the three etch times. A comparison of the three etch processes shows that increase in etch time reduces texture density leaving relatively larger features at longer etch times. The depth of the etched structures varies from ~ 0.5-1.5-μm in all three cases.

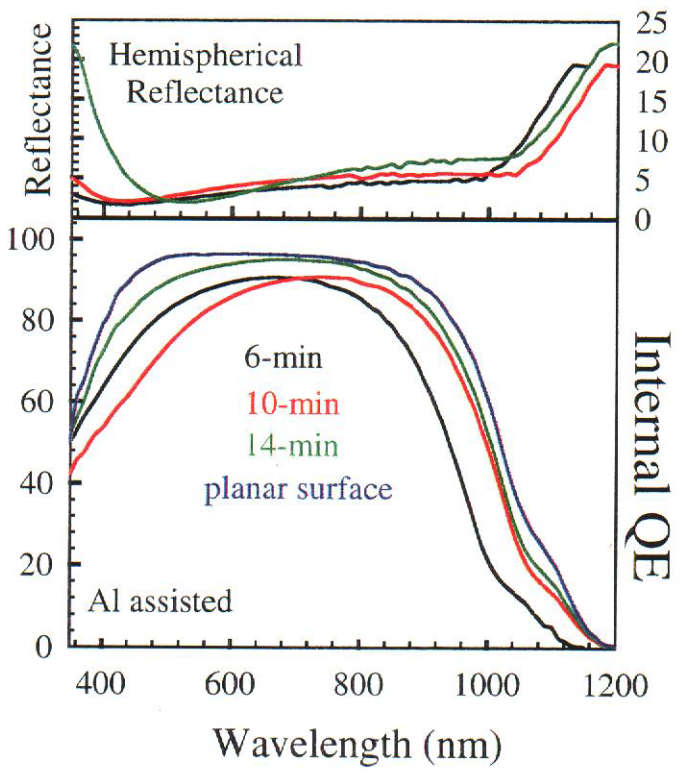

Figure 14. IQE and hemispherical reflectance measurements as function of RIE etch times.

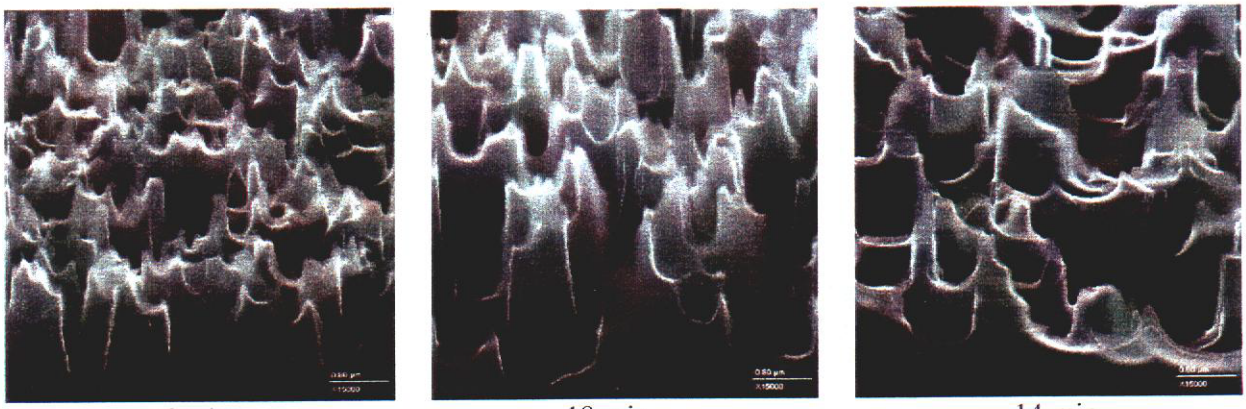

6-min 10-min 14-min

Figure 15. SEM pictures of Al-assisted random RIE textured profiles as a function of etch time, the length scale on both SEM pictures is 0.8 μm.

In order to improve IQE response, we investigated both KOH and nitric damage removal treatments. Figure 16 shows planar and textured hemispherical reflectance and IQE responses of the 10-min RIE texturing process followed by 360-sec KOH etching to remove the surface damage. A comparison of planar and textured surface responses shows that the KOH DRE has improved IQE response relative to RIE-textured surfaces without

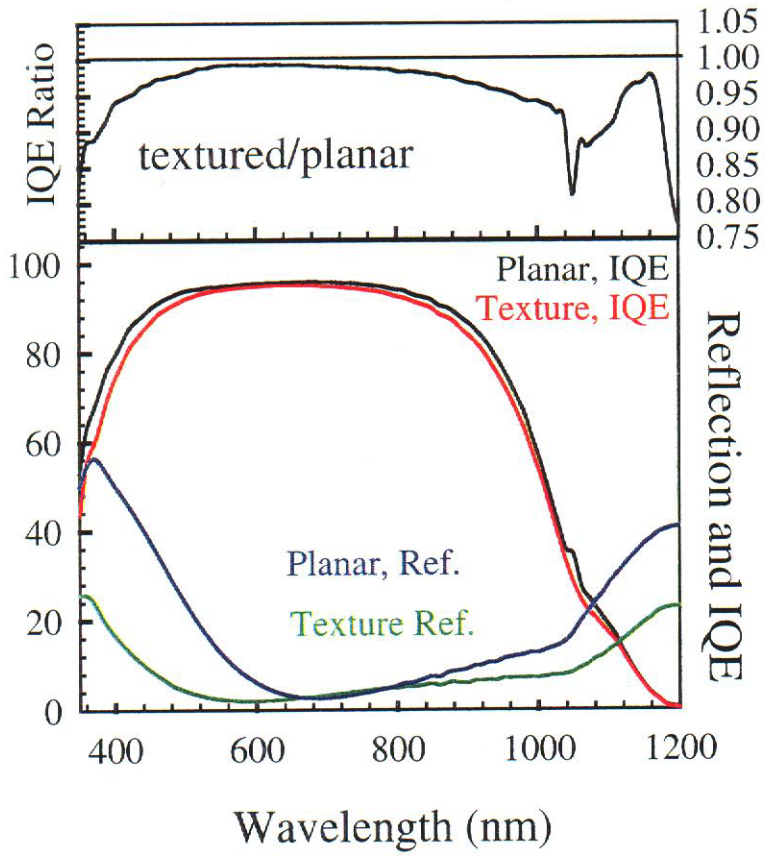

Figure 16. IQE, hemispherical reflectance and IQE ratio measurements for planar and KOH-treated 10-min RIE-textured surfaces.

DRE. However, the overall IQE is lower than the planar region over the entire spectral range. The solar-weighted surface reflectance of the textured surface at 5.1 % is still significantly lower than the planar surface (~ 11.8 %), and is comparable to the 10-min RIE surface (~ 4.4 %) shown in Figure 14. Figure 17 shows the SEM pictures of the KOH-treated random RIE-textured surfaces. It is seen that KOH etch has removed all the fine texture, i.e., surface features in 50-100-nm range. Also, average separation between random features has increased without significant variations in etched depths.

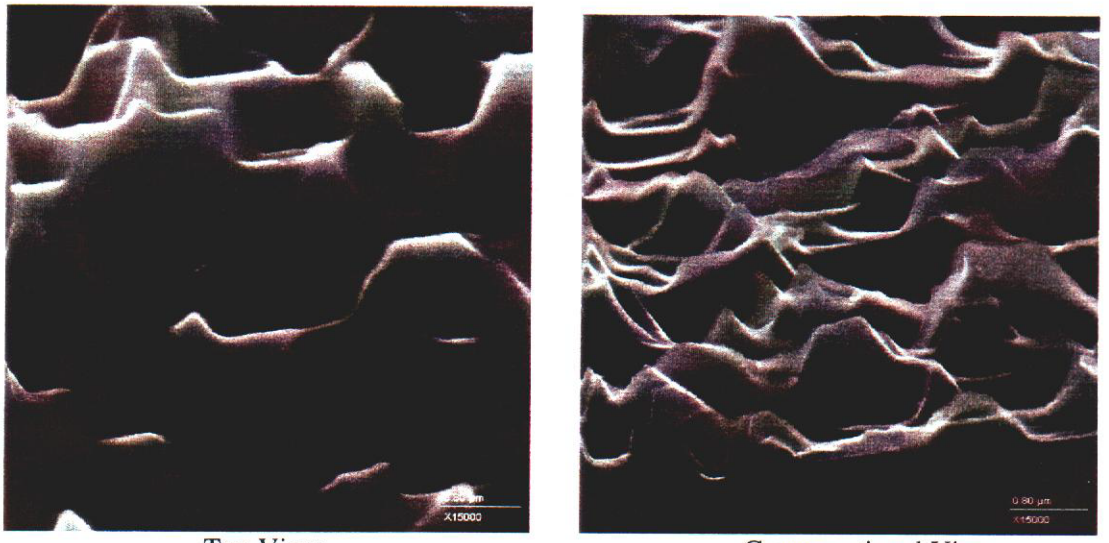

Top View Cross-sectional View

Figure 17. SEM pictures of 10-min Al-assisted random RIE textured profiles followed by 300-sec KOH etch, the length scale on both SEM pictures is 0.8 μm.

For the 14-min etch process, we also evaluated the nitric DRE process. Figure 18 shows the IQE and reflectance measurements of the planar and textured surfaces. Planar and textured IQE comparison in Figure 18 shows that nitric treatment has improved IQE response in 640-1200-nm spectral region. The IQE ratio shows a maximum enhancement of ~ 1.8 at λ ~ 1180 nm. The solar-weighted reflectance from nitric-etched surface at ~ 6.3 % is slightly higher than the KOH-treated surface. Figure 19 shows the SEM pictures of the nitric-treated random RIE-textured surfaces. It is seen that nitric etch has removed almost all the fine texture, also the average separation between individual features appears to be larger than nitric DRE /Si-cathode texture process. Finally, in Figure 20, we have plotted the I-V measurements under one-sun illumination for the five cells shown in Figures 8, 10, and 12. Comparison of cell parameters shown in Table 2 demonstrates that all cell parameters improve as etch times increase. A comparison of the two DRE processes shows that the nitric DRE is superior to the KOH.

3c. CONDITIONED TEXTURING ON CATHODE-2

The conditioned texturing process has been described in section 1; here we present its solar cell performance. For this texture process, the RIE etch time was kept constant at 15 minutes, while varying nitric DRE time from 10 to 30 seconds. Figure 21 shows the IQE and hemispherical reflectance measurements as a function of DRE time. We notice that for this texture process, the spectral reflectance is relatively insensitive to DRE etch times of 10-30 seconds. The solar-weighted reflectance varies from 5.2 %, 5.6 %, and 5.5 % at etch times of 10, 20 and 30 seconds respectively. For this texture/DRE process, the 20-sec DRE results in IQE comparable, or larger than the planar surface in the short wavelength region. In the long wavelength, similar IQE improvement is observed for each of the three etch times. Figure 22 shows SEM pictures of random RIE textured profiles for the three etch times. A comparison of the three structures shows that increase in etch time from 10 to 30 seconds reduces texture density leaving relatively larger features. The depth of the etched structures varies from ~ 0.5-1.5-μm in all three cases.

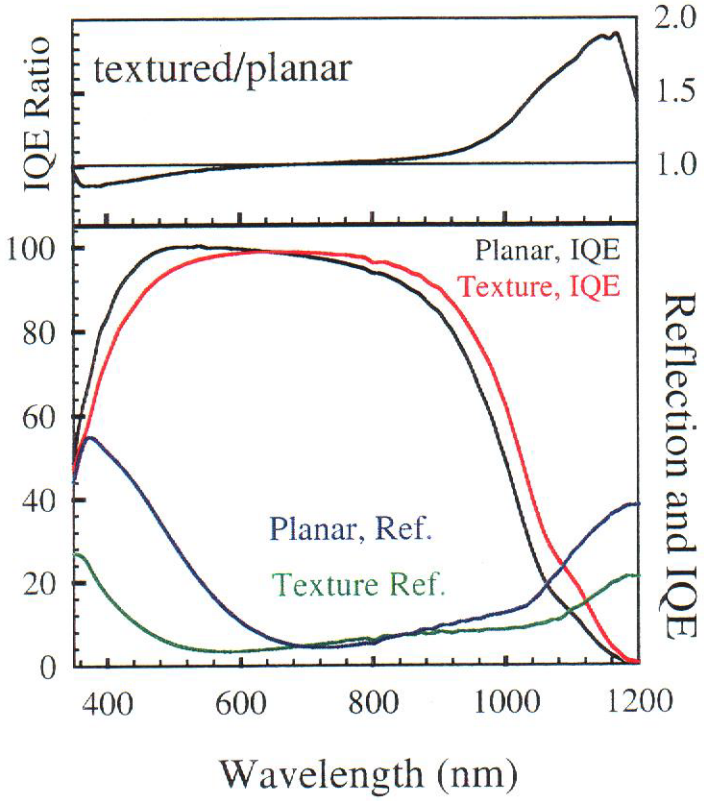

Figure 18. IQE, hemispherical reflectance and IQE ratio measurements for planar and nitric-treated 14-min RIE-textured surfaces.

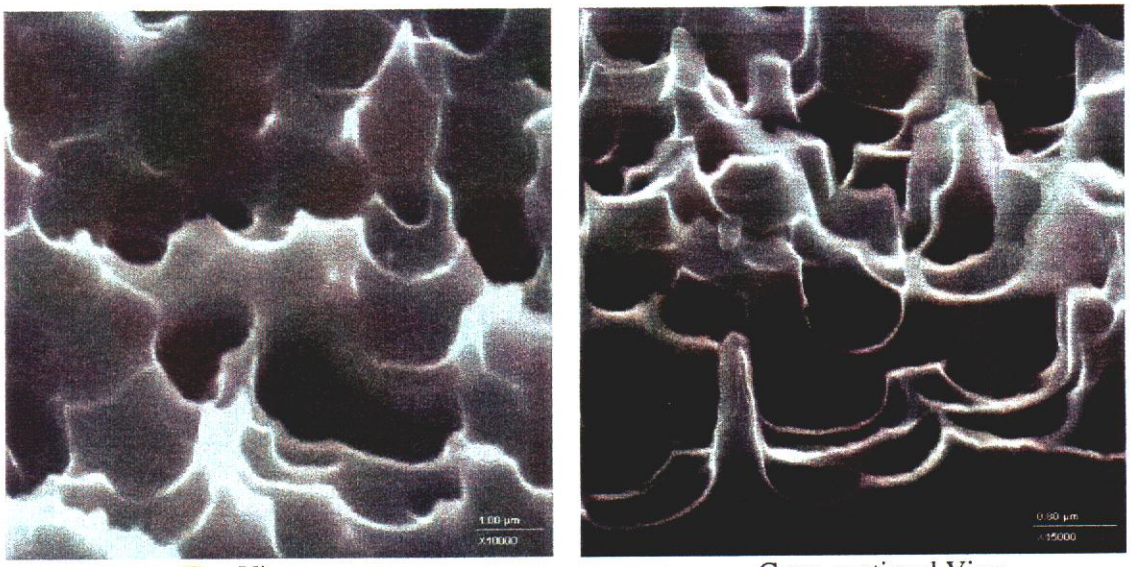

Top View

Cross-sectional View

Figure 19. SEM pictures of 14-min random RIE textured profiles followed by 10-sec nitric etch, the length scales are 1.0 and 0.8 μm respectively for the top and cross-sectional SEM pictures.

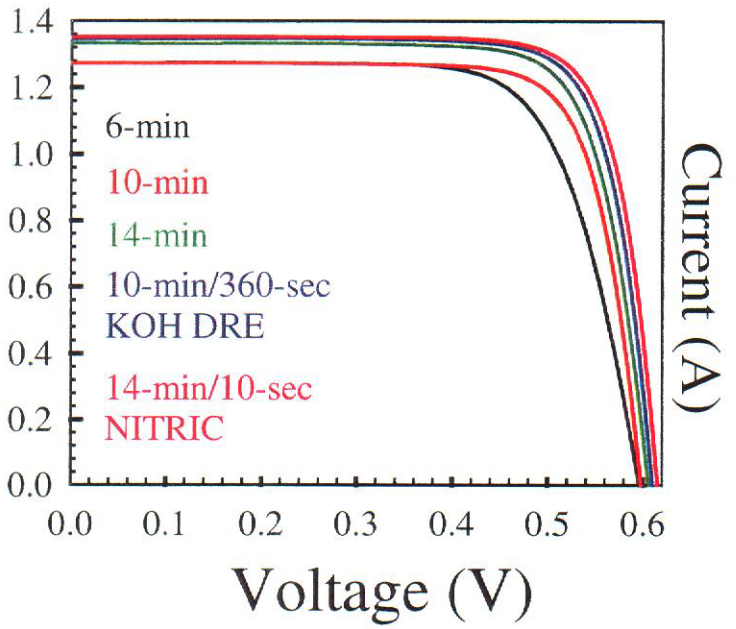

Figure 20. I-V measurements under one-sun illumination for the random RIE textured, KOH and nitric-etched solar cells.

TABLE 2. SOLAR CELL PARAMETERS OF Al-ASSISTED TEXTURE WITH AND WITHOUT DREs

Cell description	Efficiency (%)	Open-circuit voltage (V)	Short-circuit current (A)	Fill factor
6-min RIE	13.12	0.596	1.281	0.723
10-min RIE	14.25	0.605	1.337	0.766
14-min RIE	15.14	0.606	1.349	0.775
10-min RIE+360-sec KOH	15.49	0.610	1.356	0.788
14-min RIE+10-sec NITRIC	15.82	0.615	1.362	0.793

The role of the nitric DRE duration is better clarified by plotting the texture-to-planar IQE ratio for the three etch times as shown in Figure 23. We notice that for the 20-sec etch time, the IQE ratio is > 1 in both the UV and near IR regions. A maximum enhancement of ~ 1.4 is observed at λ ~ 1050 nm. For both 10 and 30-second etch times, the IQE ratios are only slightly lower relative to the 20-sec etch process. Since the 20-sec etch time shows UV IQE response superior to the planar surface, we have also compared it to the IQE response of random, wet-chemically-textured surfaces. Figure 24 shows the IQE and reflectance measurements from the RIE and wet-chemically textured surfaces, their IQE ratio is also plotted. It is seen that the wet-chemically etched surface with solar-weighted reflectance of 4.6 % has higher UV reflectance and slightly lower reflectance in the 520-1050-nm spectral region. The IQE ratio shows that the RIE the textured surface exhibits superior performance in the 350-450-nm and 880-1080-nm spectral regions. In most of the visible region, IQE ratio is unity, with wet-etch IQE superior to the RIE-texture in 1080-1180-nm spectral region. Figure 25 shows the SEM profiles of the wet-chemically etched textured surfaces. The chemically etched profiles are predominantly pyramidal-shaped with average separation of ~ 0.4-1.3 μm at depths varying from ~ 0.5-1.0 μm.

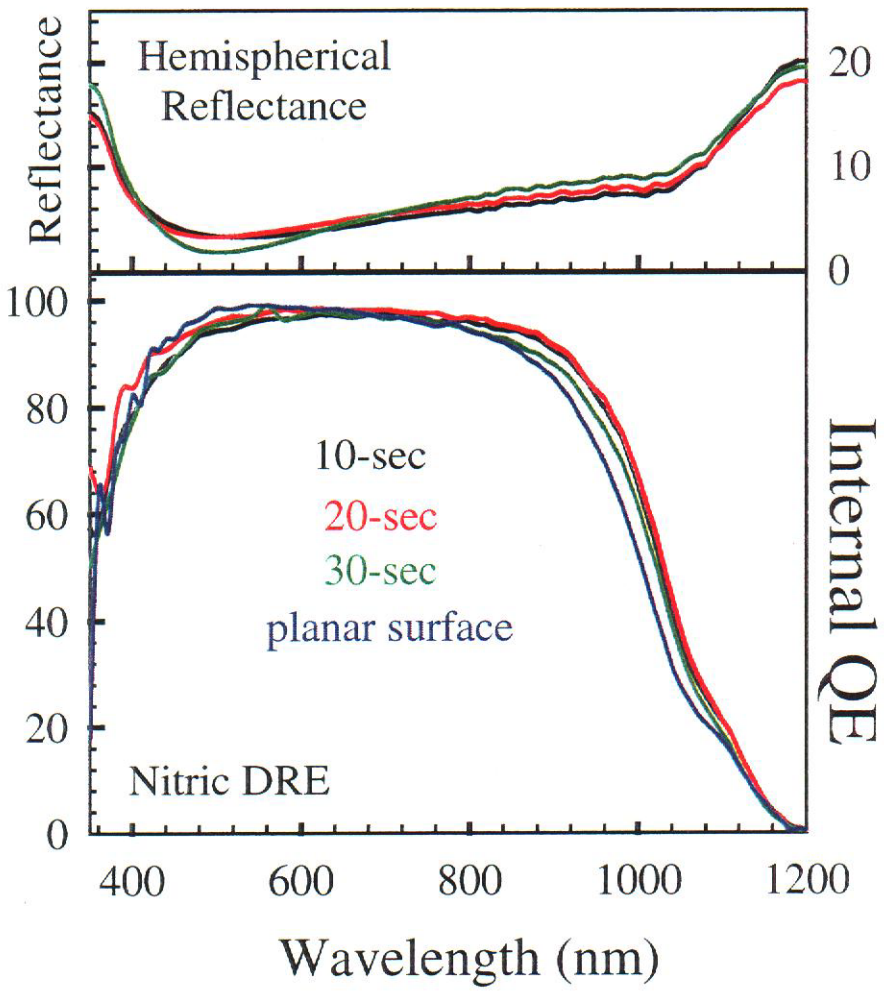

Figure 21. IQE and hemispherical reflectance measurements as function of nitric DRE etch times.

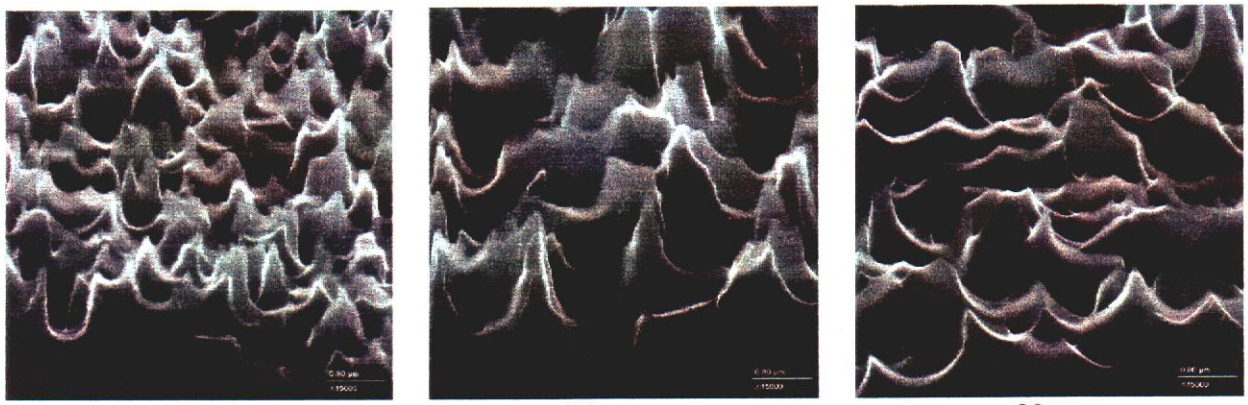

10-sec 20-sec 30-sec

Figure 22. SEM pictures of un-assisted random RIE textured profiles as a function of etch time, the length scale on both SEM pictures is 0.8 μm.

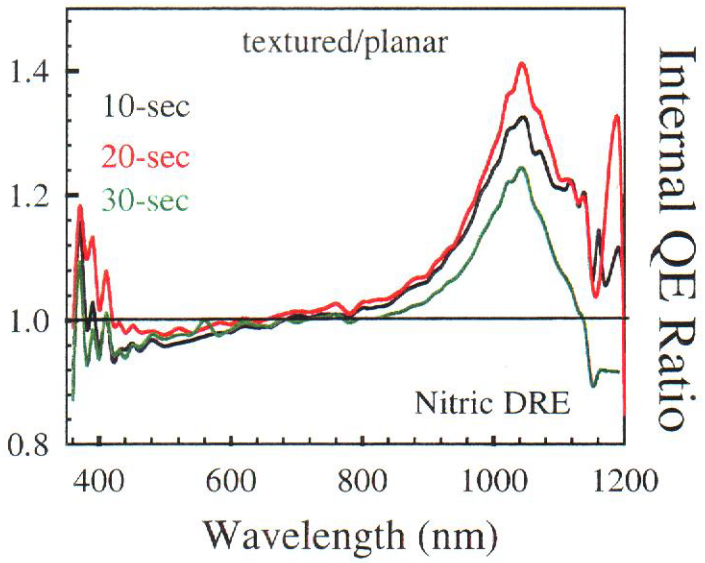

Figure 23. IQE ratio measurements for un-assisted texture process with nitric DRE treatments.

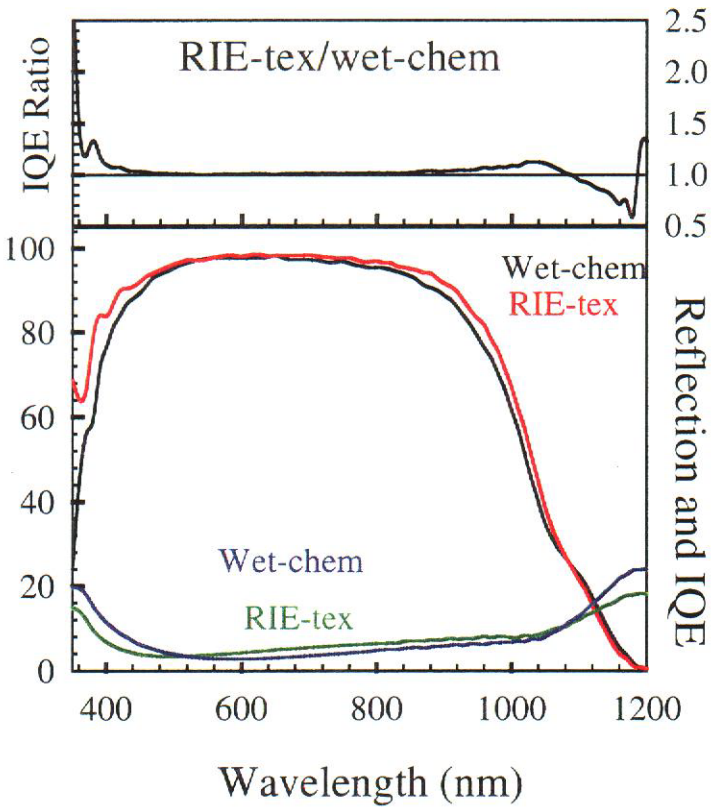

Figure 24. IQE, hemispherical reflectance and IQE ratio measurements for wet-textured and nitric-treated random RIE-textured surfaces.

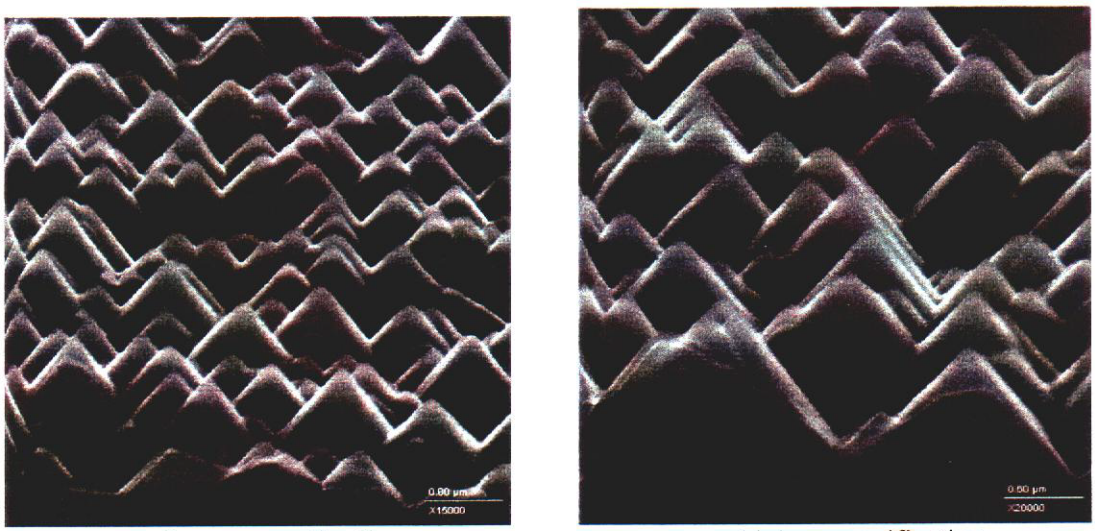

lower magnification higher magnification

Figure 25. SEM pictures of random, wet-chemically textured surfaces, the length scale on the lower and higher magnification SEM pictures are 0.8 μm and 0.6 μm respectively

Finally, in Figure 26, we have plotted the I-V measurements under one-sun illumination for the five cells shown in Figures 21 and 24. Table 3 summarizes some of the critical cell parameters. Comparison of cell parameters shows an overall improvement as etch times increase. For all textured surfaces, the overall performance is superior to the planar surface. For the RIE texture process, significant improvement is seen as etch time is increased from 10 seconds. Cell performances are similar for DRE times of 20 and 30 seconds. The wet-chemically etched surface exhibits superior response in comparison with the RIE-textured surfaces.

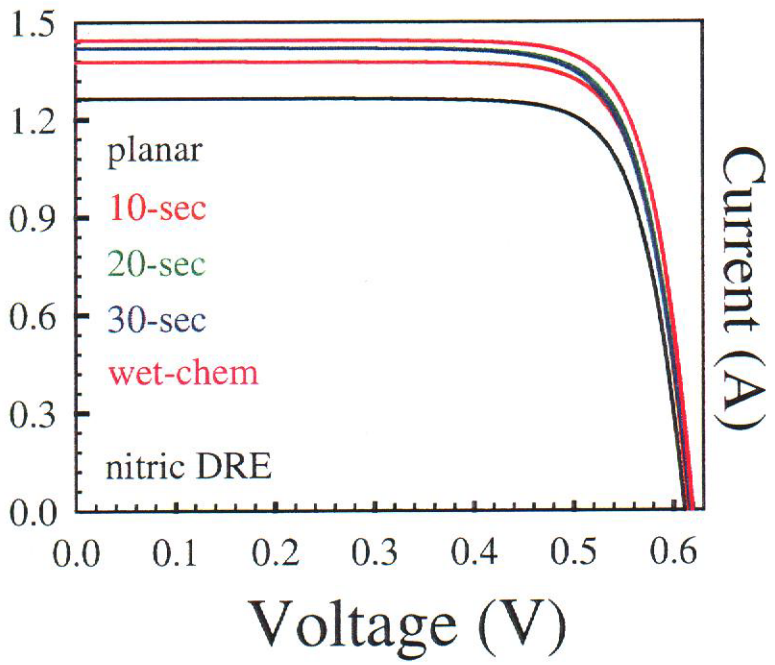

Figure 26. I-V measurements under one-sun illumination for the planar, random RIE and wet-chemically textured solar cells.

TABLE 3. SOLAR CELL PARAMETERS FOR PLANAR, UN-ASSISTED AND WET-TEXTURE PROCESSES

Cell description	Efficiency (%)	Open-circuit voltage (V)	Short-circuit current (A)	Fill factor
Planar	14.5	0.611	1.269	0.786
10-sec Nitric DRE	16.07	0.615	1.390	0.787
20-sec Nitric DRE	16.48	0.617	1.434	0.781
30-sec Nitric DRE	16.43	0.618	1.439	0.774
Random, Wet-chemical	16.96	0.619	1.452	0.792

4. ANALYSIS OF INTERNAL QUANTUM EFFICIENCY MEASUREMENTS

In the previous section, IQE measurements from six texture processes were presented. In order to understand their relative merits, we have plotted all six IQE ratios and hemispherical reflectances in Figures 27 and 28. The salient features of the IQE ratio measurements in Figure 27 can be summarized as follows:

i. Chemically-etched and nitric DRE on cathode-1 have almost identical IQE response over the entire spectral region with maximum enhancement of ~ 1.5 at λ ~ 1200 nm,
ii. Conditioned nitric DRE and KOH DRE on cathode-1 have similar IQE response with maximum enhancement of ~ 1.5 at λ ~ 1000 nm,
iii. The Al-assisted RIE with nitric DRE has a behavior similar to that described in (i) above, except that it has higher enhancement of ~ 1.8 at the same wavelength, and
iv. The Al-assisted RIE with KOH DRE shows no IQE enhancement.

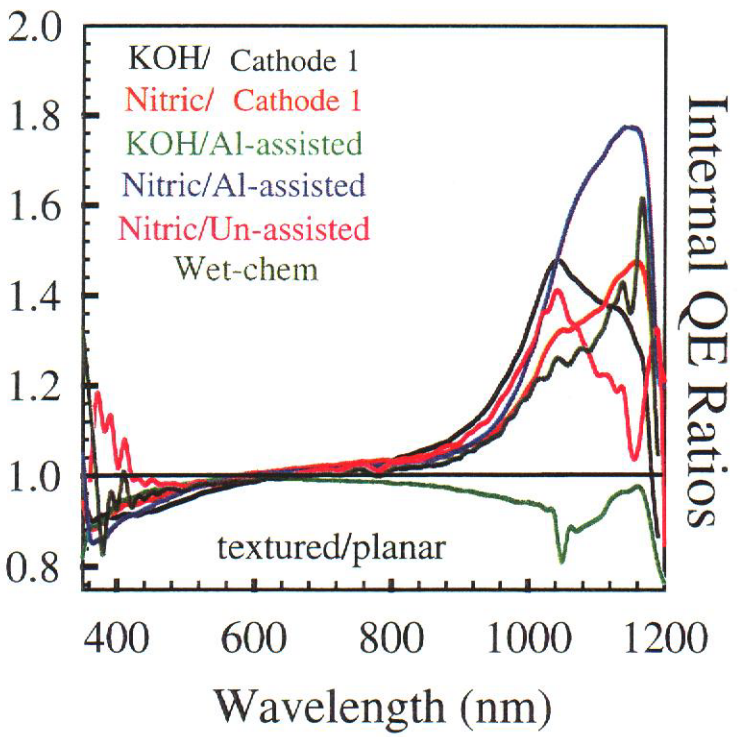

Figure 27. IQE ratios from five random RIE-textured surfaces with KOH and DRE treatments (for reference the IQE ratio from wet-chemically etched surface is also plotted).

The salient features of the hemispherical reflectance measurements shown in Figure 28 can be summarized as follows:

i. Nitric DREs on conditioned and cathode-1 RIE processes have similar reflectance response, however, their near IR IQE response is significantly different,
ii. The chemically-etched surface has UV reflectance similar to RIE-textures in (i), however, its long wavelength reflectance is lower,
iii. The Al-assisted RIE with nitric and KOH DREs both have almost identical reflectance response, however, their IQE responses are different, and
iv. The lowest reflection is observed for KOH DRE on cathode-1 RIE process, its IQE response is similar to the conditioned texture process.

These results show that there appears to be no correlation between the measured reflectance response of a texture process, and its IQE response. The key solar cell parameters from the five textured surfaces are summarized in Table 4. Comparison of the five RIE-texturing processes demonstrates the superiority of conditioned texturing process combined with nitric DRE treatment.

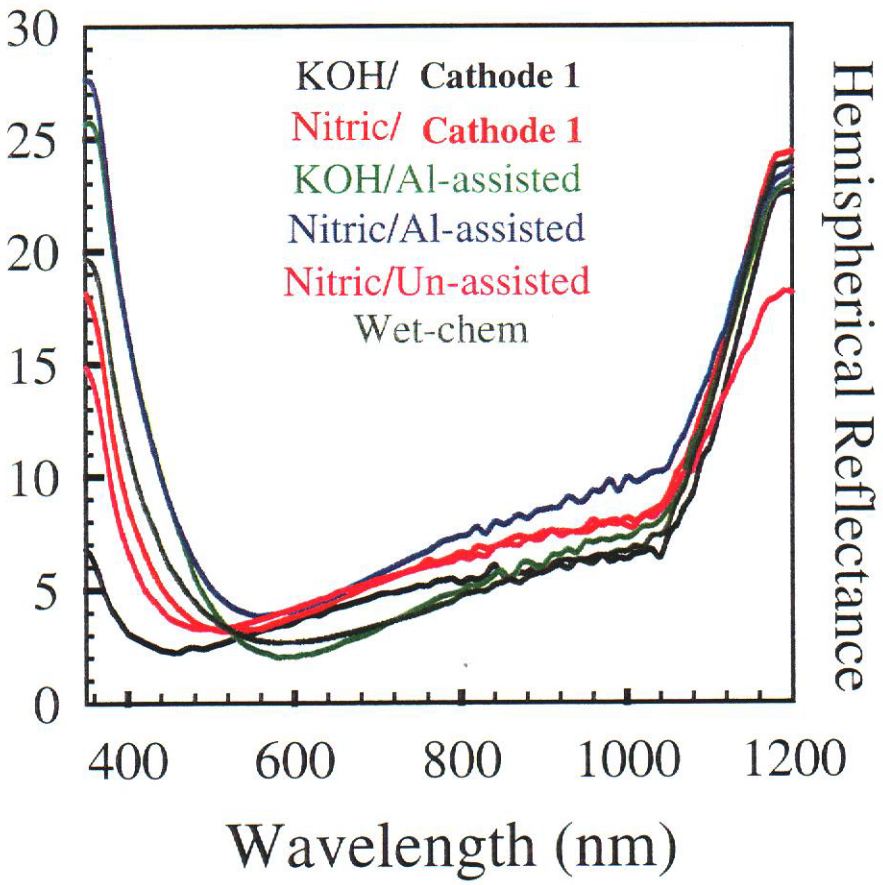

Figure 28. Hemispherical reflectance measurements from five random RIE-textured surfaces with KOH and DRE treatments (for reference the reflectance from wet-chemically textured surface is also plotted).

TABLE 4. SOLAR CELL PARAMETERS FOR SIX TEXTURE PROCESSES

Cell description	Efficiency (%)	Open-circuit voltage (V)	Short-circuit current (A)	Fill factor
Cathode-1, KOH DRE	15.27	0.609	1.273	0.764
Cathode-1 Nitric DRE	14.74	0.588	1.378	0.765
Al-assisted, KOH DRE	15.49	0.610	1.356	0.788
Al-assisted, Nitric DRE	15.82	0.615	1.362	0.793
Conditioned, Nitric DRE	16.48	0.617	1.434	0.781

4a. DIFFRACTIVE COUPLING OF LIGHT INTO SEMICONDUCTOR

In order to understand the IQE enhancement in near IR region, it is useful to briefly review diffractive optics. A random surface represents a superposition of a number of grating structures supporting a wide distribution of periods, depths, and profiles. Light incident on such a surface is randomly scattered into various diffraction orders both in air and inside the semiconductor substrate. The distribution of energy in these obliquely propagating diffraction orders is a complex function of many parameters including wavelength, incident angle, period, profile, and depth. A simple case is illustrated in Figure 29, which shows a single grating etched into the top surface of a Si wafer. A beam of light at wavelength λ is normally incident the grating surface defined by period d, linewidth l, and depth h. The period is chosen such that there are no diffraction orders in air, i.e., $\lambda/d > 1$. Inside the semiconductor, first and second diffraction orders are propagating due to its higher refractive index n,

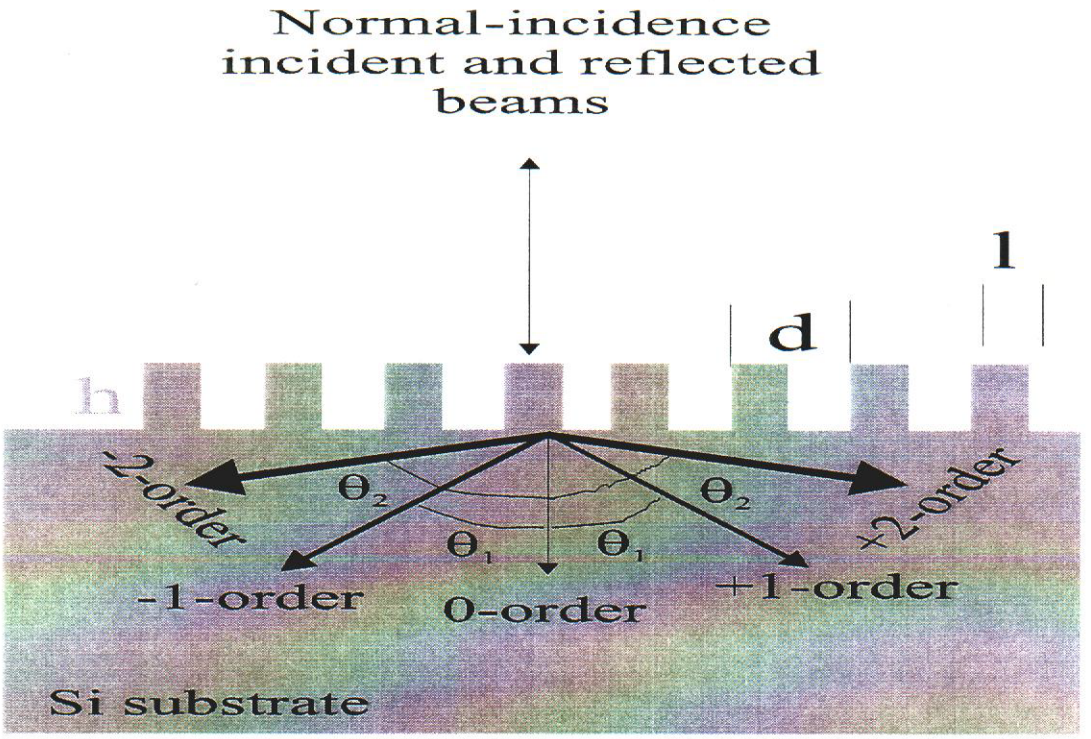

Figure 29. Diffractive optical coupling of light into the semiconductor for a single grating surface.

i.e., $2^* \lambda/(n^*d) < 1$. We can calculate the propagation angles inside Si using the grating equation. Figure 30 shows the propagation angles inside Si of normally incident beams for four grating periods. We notice that for periods between 0.27-0.33-μm, first diffraction order approaches angles ~ 90° at λ ~ 960, 1070, and 1160 nm. For larger grating periods of ~ 0.4 and 0.5-μm, first diffraction orders approach ~ 40° and 30° at λ ~ 1000 nm.

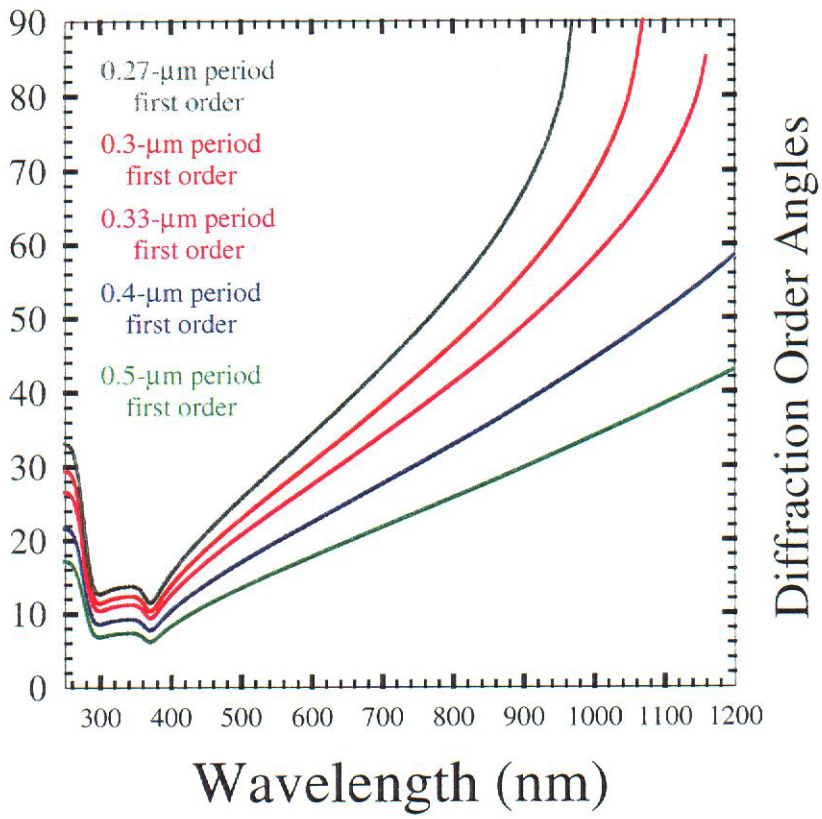

Figure 30. Angular variation of transmitted diffraction orders as a function of wavelength.

The distribution of energy into transmitted diffraction orders is a complex function of many variables including polarization, angle, profile, period, and depth. Using GSOLVER™ software, we have calculated diffraction efficiencies of the first and second diffraction orders for two profiles as shown in Figure 31. It is seen that for TM-polarization, energy distribution for both profiles is a periodic function of grating depth. For these calculations, light at λ ~ 1.0 μm was normally incident and a 75 % duty cycle for rectangular profile grating was assumed. The triangular profile was assumed to be symmetric. These 1D calculations demonstrate ~ 80-100 % coupling of incident light into obliquely propagating diffraction orders for grating depths varying from ~ 0.25-1.5 μm. Since the random RIE-textured profiles are more complex 2D structures, a better picture of diffractive coupling requires 2D modeling of grating structures.

Since the material properties of the wafer are isolated by taking IQE ratios from adjacent planar and textured regions on the same wafer, the enhanced near IR IQE can be explained by increased light coupling into the obliquely propagating orders. Due to long near IR absorption lengths in Si, the normally propagating zero-order beam in the absence of a diffractive scattering surface is absorbed deep into the bulk region. A significant fraction of these photo-generated electron-hole pairs are lost to bulk recombination. However, the random RIE-textured surface couples light more effectively into obliquely propagating orders, thus, creating electron-hole pairs closer to the surface and reducing their recombination probability.

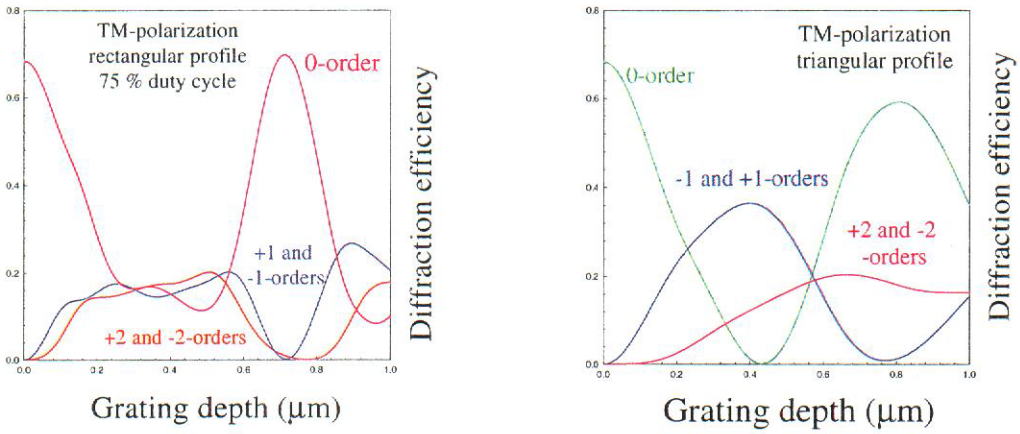

Figure 31. Calculated-coupling efficiencies of first and second diffraction orders for 0.65-μm period grating with rectangular and triangular profiles.

We have investigated the IQE response of various grating structures as part of an effort aimed at an understanding of the IQE enhancement in near IR region. Figure 32 shows the IQE ratio of grating/planar regions of the same wafer for rectangular and triangular profiles at a period of ~ 0.5 μm. We notice that both these profiles show peak enhancement at λ ~ 1050 nm, the rectangular profile IQE enhancement is ~ 2.6, the triangular profile ~ 1.5. The IQE enhancement response from these 1D grating structure is similar to that observed by the un-assisted and cathode-1 RIE texturing processes, although rectangular profile has significantly higher enhancement in near IR IQE. Since the random RIE-textured profiles support structures in 0.3-1.0 μm range, it is probable a fraction of incident energy is coupled into the obliquely propagating diffraction orders. This explains the enhancement in near IR IQE response.

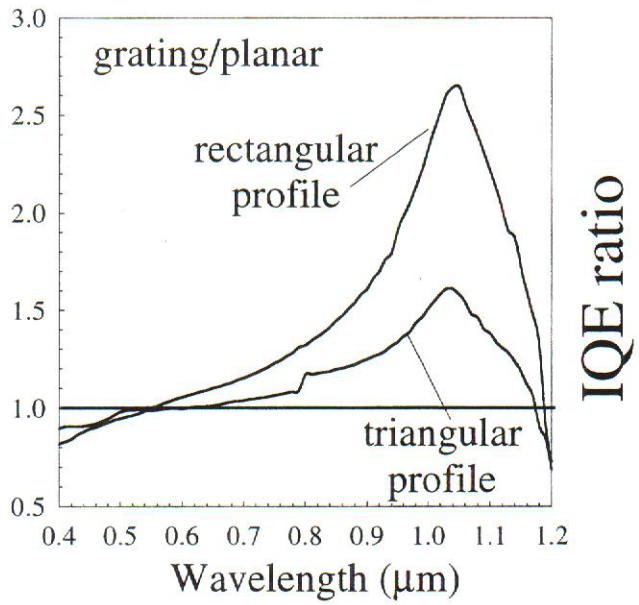

Figure 32. IQE ratio from grating and planar regions of for the same period, but different profiles.

5. SUMMARY AND FUTURE WORK

We have developed a unique texture control process based on metal-catalytic influence of the plasma texturing process. This random texture tunability has led to an optimum profile for the optimum solar cell performance. Most of the randomly textured features not only reduce surface reflection, but also enhanced near IR internal quantum efficiency response. The IQE enhancement is believed to originate from enhanced diffractive coupling into obliquely propagating first and second transmitted diffraction orders inside Si. Further optimization is required in:

a) DRE treatments consistent with lowest reflection losses,
b) Improvement in RIE texturing process without DRE treatments, and
c) Extension of the texturing process to large area multi-crystalline Si substrates.

6. REFERENCES

1. *Fundamentals of Solar cells: Photovoltaic Solar Energy Conversion*, Alan L. Fahrenbruch and Richard H. Bube, Academic Press (1983).
2. E. Yablonovitch, J.O.S.A. **72**, 899 (1982).
3. H. W. Deckmann, C. R. Wronski, H. Witzke, and E. Yablonovitch, Appl. Phys. Lett. **42**, 968 (1983).
4. S. Bastide, A. Albu-Yaron, S. Strehlke, C. Levy-Clement, Solar Energy Materials & Solar Cells **57**, 393 (1999).
5. H. Nussbaumer, G. Willeke, E. Bucher, J. Appl. Phys. **75**, 2202 (1994).
6. H. G. Craighead, R. E. Howard, J. E. Sweeney, and D. M. Tenant, J. Vac. Sci. Technol. **20**, 316 (1982).
7. D. S. Ruby and Saleem H. Zaidi, "Metal-catalyst technique for texturing silicon solar cells", US Patent filed on Aug. 9, 2000.
8. W. H. Southwell, J. Opt. Soc. Am. **A 8**, 549 (1991).
9. Saleem H. Zaidi, Sandia Report, SAND2000-0919, April 2000.

7. ACKNOWLEDGEMENTS

We would like to thank Sandia National Laboratories for their financial and technical support during the course of this work. In particular, we would like to thank Dr. Douglas S. Ruby, James M. Gee, Jeannette Moore, Bev Silva, and Bob Ellis of Sandia for their help during the course of this project. We would also like to thank the Center for High Technology Materials at the University of New Mexico for use of their clean room facilities. Many thanks are also to Richard Marquardt and Sam McCormack of Gratings, Inc. for their assistance.

DISTRIBUTION

Keith Matthei
GT Solar Technologies
472 Amherst Street
Nashua, NH 03063

Gary Stevens
Matrix Solar
7500 Meridian Place
Albuquerque, NM 87121

Mike Nowland
Spire Corporation
One Patriots Park
Bedford, MA 01810

Steve Hogan
Spire Corporation
One Patriots Park
Bedford, MA 01810

Juris Kalejs
ASE Americas, Inc.
Four Suburban Park
Billerica, MA 01821-3980

Mark Rosenblum
ASE Americas, Inc.
Four Suburban Park
Billerica, MA 01821-3980

James Rand
AstroPower
Solar Park
Newark, DE 19716-2000

Chandra Khattak
Crystal Systems
27 Congress Street
Salem, MA 01970

Mohan Narayanan
Solarex Corporation
630 Solarex Court
Frederick, MD 21701

John Wohlgemuth
Solarex Corporation
630 Solarex Court
Frederick, MD 21701

Ted Ciszek
National Renewable Energy Lab
1617 Cole Blvd.
Golden, CO 80401-3393

Bhushan Sopori
National Renewable Energy Lab
1617 Cole Blvd.
Golden, CO 80401-3393

Jack Hanoka
Evergreen Solar, Inc.
211 Second Avenue
Waltham, MA 02154

Andrew Gabor
Evergreen Solar, Inc.
211 Second Avenue
Waltham, MA 02154

Theresa Jester
Siemens Solar Industries
P. O. Box 6032
Camarillo, CA 93011

Dan Meier
Ebara Solar, Inc.
811 Route 51 South
Large, PA 15025

Ajeet Rohatgi
Georgia Institute of Technology
777 Atlantic Drive, EE
Atlanta, GA 30332

Jeffrey Mazer
US Department of Energy, EE-11
1000 Independence Ave., SW
Washington, DC 20585

Richard King
US Department of Energy, EE-11
1000 Independence Ave., SW
Washington, DC 20585

Richard Swanson
SunPower Corporation
430 Indio Way
Sunnyvale, CA 94086

Pierre Verlinden
SunPower Corporation
430 Indio Way
Sunnyvale, CA 94086

Saleem Zaidi
Gratings, Inc.
7104 Jefferson N.E.
Albuquerque, NM 87109

Hong Hou
EMCORE Photovoltaics
10420 Research Rd. S.E.
Albuquerque, NM 87123

Richard King
Spectrolab, Inc.
12500 Gladstone Avenue
Sylmar, CA 91342-5373

Frank Ho
Tecstar, Inc.
15251 E. Don Julian Road
City of Industry, CA 91745

Vahan Garboushian
Amonix, Inc.
3425 Fujita Street
Torrance, CA 90505

Tihu Wang
National Renewable Energy Lab
1617 Cole Blvd.
Golden, CO 80401

Bob McConnell
National Renewable Energy Lab
1617 Cole Blvd.
Golden, CO 80401

0752	Doug Ruby, 6218
0752	James Gee, 6201
0752	David King, 6218
0753	Joe Tillerson, 6218
0753	PV Library (5 copies)
0899	Technical Library, 9616 (2 copies)
0619	RA Desk, 9612 for DOE/OSTI
9018	Central Technical Files, 8945-1